Advances in Aircraft and Spacecraft Science, *Vol. 9, No. 1 (2022) 69-93*
https://doi.org/10.12989/aas.2022.9.1.069

Isogeometric analysis of FG polymer nanocomposite plates reinforced with reduced graphene oxide using MCST

Amir Farzam*[1,2] and Behrooz Hassani[3]

[1]Department of Civil Engineering, Ferdowsi University of Mashhad, Mashhad, Iran
[2]Department of Aerospace and Ocean Engineering, Virginia Polytechnic Institute and State University, Blacksburg, VA 24061, USA
[3]Department of Mechanical Engineering, Ferdowsi University of Mashhad, Mashhad, Iran

(Received August 6, 2021, Revised January 26, 2022, Accepted January 27, 2022)

Abstract. Reduced graphene oxide (rGO) is one of the derivatives of graphene, which has drawn some experimental research interests in recent years however, numerical research studying the mechanical behaviors of composites made of rGO has not been taken into consideration yet. The objective of this research is to investigate the buckling, and free vibration of functionally graded reduced graphene oxide reinforced nanocomposite (FG rGORC) plates employing isogeometric analysis (IGA). The effective Young's modulus of rGORC is determined based on the Halpin-Tsai model. Four different FG distribution types of rGO are considered varying across plate thickness. Besides, the refined plate theory is used based on Reddy's third-order function. To capture the size effect, modified couple stress theory (MCST) is employed. A comprehensive study is provided examining the effect of various parameters including rGO weight fraction, FG distribution types, boundary conditions, material length scale parameter, etc. Our obtained results show that the addition of only 1% of uniformly distributed rGO into epoxy plates leads to the fundamental frequency and critical buckling load 18% and 39% higher than those of pure epoxy plates, respectively.

Keywords: Buckling; Free Vibration; Isogeometric Analysis (IGA); Modified Couple Stress Theory (MCST); Reduced Graphene Oxide (rGO)

1. Introduction

In the last decade, graphene and its derivatives have been widely investigated due to their outstanding electrical and mechanical properties. There can be found much research in the literature devoted to analyzing the mechanical behaviors of composites made of carbon nanotubes (CNTs) (Zhang *et al*. 2016, Farzam and Hassani 2019), graphene platelets (GPLs) (García-Macías *et al*. 2018, Song *et al*. 2018) and graphene oxide (GO) (Zhang *et al*. 2018). CNTs and GPLs tend to easily agglomerate and restack in the matrix, which significantly weakens the mechanical strength of composites. Therefore, to resolve such problems GO could be used. GO is structurally similar to graphene and a promising candidate for reinforcing composites. By oxidizing, the interlayer distance between graphite layers increases and so GO can be easily exfoliated compared to graphite or GNPs due to the Vander Waals forces. Also, functional groups of GO can be helpful and effective on the interfacial interaction, distribution of GNPs as well as load transfer between GO monolayers and

*Corresponding author, Ph.D. Student, E-mail: amfarzam@vt.edu

http://www.techno-press.org/?journal=aas&subpage=7 ISSN: 2287-528X (Print), 2287-5271 (Online)

matrix (Rafiee *et al*. 2010).

GO can be thermally or chemically reduced to graphene so-called reduced graphene oxide (rGO). In other words, rGO is obtained by reducing or removing the functional groups of GO. This process can partially restore mechanical and electrical properties. For instance, GO behaves as a soft structure, while rGO seems very hard (Huang *et al*. 2018). A schematic illustration of the fabrication process for rGO is depicted in Fig. 1. Reduced graphene oxide sheets have lateral dimensions of 0.1-5 μm with an elastic modulus of 0.25±0.15 TPa (Gómez-Navarro *et al*. 2008). Robinson *et al*. (2008) reported 0.185 TPa for Young's modulus of rGO thin films. Li *et al*. (2015a) reported the average sizes of reduced graphene and non-covalently functionalized graphene with poly(sodium 4-styrene sulfonate) (PSS) are smaller than GOs. They estimated the aspect ratio of PSS graphene to be 1000-2000. Regarding the epoxy polymer matrix and rGO, some experimental research can be found in the literature. Starkova *et al*. (2013) investigated the thermo-mechanical properties of the epoxy resin matrix filled with thermally reduced graphene oxide (TRGO) and multi-wall carbon nanotubes (MWCNTs). They showed the improvement of the thermo-mechanical properties of the neat epoxy is higher for the TRGO compared to the MWCNTs. Yousefi *et al*. (2013a) prepared rGO/waterborne epoxy composites using hydrazine and *in situ* polymerization. They reported the formation of composites with a self-aligned layered structure and highly anisotropic properties. TK *et al*. (2014) made microwave exfoliated reduced graphene oxide (MERGO) from natural graphite via *in situ* polymerization. Olowojoba *et al*. (2016) developed a facile method to prepare epoxy resin composites containing rGO. They recorded improvements in thermal conductivity, storage modulus, and tensile modulus. There are also other experimental research studying the effects of rGO on ceramics (Ramirez *et al*. 2014, Xia *et al*. 2015, Belmonte*et al*. 2016, Hanzel*et al*. 2017, Shin and Hong 2014, Lee *et al*. 2014, Walker *et al*. 2011, An *et al*. 2016), poly(methyl methacrylate) (PMMA) (Zeng *et al*. 2012, Potts *et al*. 2011, Gong *et al*. 2016, Wang *et al*. 2012, Pham *et al*. 2012, Mishra *et al*. 2014, Ji *et al*. 2014, Tripathi *et al*. 2013) poly(methyl methacrylate), poly(vinylidene fluoride) (PVDF) (Maity *et al*. 2016), polyimide (PI) (Kong *et al*. 2012), polyurethane (PU) (Yousefi *et al*. 2013b), polyvinyl alcohol (PVA) (Kashyap *et al*. 2016, Zhou *et al*. 2011), polycarbonate (PC) (Xu *et al*. 2013), polydimethylsiloxane (PDMS) (Kim *et al*. 2019), phenol formaldehyde (PF) (Sandhya *et al*. 2019), polymers (Weon 2009, She *et al*. 2014, Iqbal *et al*. 2016, Fornes and Paul 2003), aluminum (Li *et al*. 2015b, Li *et al*. 2014, Liu *et al*. 2016), concrete (Qureshi and Panesar 2019) matrices. Also, references (Zhu *et al*. 2010, Compton and Nguyen 2010) provide further reviews in terms of the properties and applications of graphene and its derivatives.

To capture the size effect, many size-dependent continuum mechanics models were suggested such as nonlocal elasticity theory (Eringen and Edelen 1972, Hosseini *et al*. 2020, Fenjan *et al*. 2020, Belmahi *et al*. 2019, Dastjerdi *et al*. 2020), nonlocal strain gradient theory (Fleck and Hutchinson 1993, Abazid *et al*. 2020, Sobhy and Zenkour 2021, Sobhy and Zenkour 2019, Dindarloo and Zenkour 2020, Miglani *et al*. 2021), modified couple stress theory (MCST) (Yang *et al*. 2002), and modified strain gradient theory (MSGT) (Lam *et al*. 2003, Akgöz and Civalek 2017). In all aforementioned theories, length scale parameters are appearing in the governing equations. These parameters could be experimentally measured. The MSGT can be obtained by reducing the number of length scale parameters from five in the strain gradient theory to three. By further simplification, one can obtain the MCST having only one length scale parameter, which leads to having much less complication in relations. Based on size-dependent continuum mechanics models, there can be found some research in the literature studying composite plates reinforced with graphene platelets (GPLs). Karami *et al*. (2019) investigated the resonance of FG composite nanoplates reinforced by GPLs using the nonlocal strain gradient theory. They concluded that the

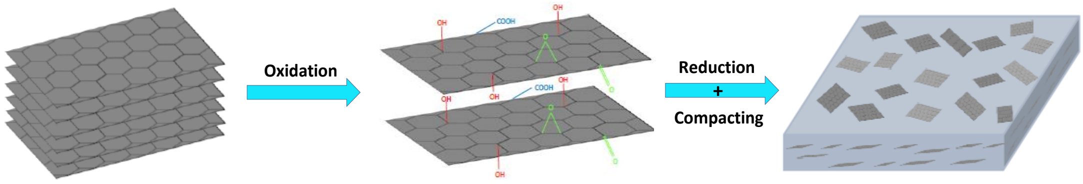

(a) Graphite (b) Graphene oxide (GO) (c) rGORC

Fig. 1 Schematic illustration of the fabrication process for reduced graphene oxide reinforced composite (rGORC) plates

increase of the nonlocal parameter results in a resonance position with approaching to lower load frequencies. Pourjabari *et al*. (2019) studied the free and forced vibration of porous GPLRC nanoplates using the MSGT. Sahmani *et al*. (2018) examined the non-linear amplitude vibration of porous GPLRC plates based on the nonlocal strain gradient theory. They used the closed-cell Gaussian-Random field scheme to determine the mechanical properties of porous materials. Thai *et al*. (2019a, b) studied the free vibration and buckling of multilayer FG GPLRC microplates based on the MCST and MSGT.

In 2005, isogeometric analysis (IGA) was introduced by Hughes *et al*. (2005) IGA employs either B-splines or Non-Uniform Rational B-Spline (NURBS) as shape functions. IGA can be used as an efficient numerical method, which can easily produce the exact geometry of problems and so IGA can solve problems with complex shapes. In recent years, IGA has been successfully used to analyze composite plate structures (Thanh *et al*. 2018, Phung-Van *et al*. 2017, 2018, 2019, Farzam and Hassani 2019a, b, c, Farzam-Rad *et al*. 2017, Saeedi *et al*. 2020, Devarajan and Kapania 2020, Kapoor *et al*. 2013, Kapoor and Kapania 2012, Devarajan and Kapania 2022) and plates reinforced by GPLs (Phung-Van *et al*. 2019, Li *et al*. 2018, Kiani 2018a, b, Thai *et al*. 2019, Nguyen *et al*. 2019).

To the best of the authors' knowledge, there is no research in the literature investigating the mechanical behaviors of functionally graded polymer nanocomposite plates reinforced by reduced graphene oxide (rGO). For the first time, the current research study provides numerical solutions for rGO composite plates. Although graphene composite structures have been widely studied, the aggregation of graphene plates is a key issue, and so the study of fabrication and analysis of rGO composites could draw attention. In what follows first, the MCST is briefly explained and then equations of the Halpin-Tsai model, as well as four different distribution types across the plate thickness, are given. After that, the displacement field of a plate based on the refined plate theory is expressed. NURBS basis functions and the formulation of a plate are briefly presented in section 4. Finally, obtained results are validated and compared with solutions available in the literature besides discussion on presented results in details.

2. Modified couple stress theory

Based on modified couple stress theory (MCST) (Yang *et al*. 2002), the strain energy can be written as

$$U = \frac{1}{2}\int \left(\sigma_{ij}\varepsilon_{ij} + m_{ij}\chi_{ij}\right)dV \tag{1}$$

where σ and ε are the stress and strain tensors. m and χ are the components of the deviatoric part of the symmetric couple stress and curvature tensors defined as (Zenkour 2018a, b, Sobhy and Zenkour 2020)

$$m_{ij} = \frac{E(z)}{(1+\nu)} l^2 \chi_{ij} \tag{2}$$

$$\chi_{ij} = \frac{1}{2}\left(\frac{\partial \theta_i}{\partial x_j} + \frac{\partial \theta_j}{\partial x_i}\right) \tag{3}$$

in which $\theta = \frac{1}{2}\mathrm{curl}(u)$ is the rotation vector, u is displacement, and l is named material length scale parameter.

By considering a rectangular plate with length a, width b, and thickness h reinforced with fillers randomly arranged on the x-y plane. Based on the Halpin-Tsai micromechanics model (Van 2001), Young's modulus E_{random} is approximated as

$$E_{random} = \frac{3}{8}E_{||} + \frac{5}{8}E_{\perp} \tag{4}$$

in which $E_{||}$ and $E_{\perp}$ are in-plane Young's modulus defined as

$$E_{||} = E_m \frac{1 + \xi_L \eta_L V_r}{1 - \eta_L V_r} \tag{5}$$

$$E_{\perp} = E_m \frac{1 + \xi_w \eta_w V_r}{1 - \eta_w V_r} \tag{6}$$

in which

$$\eta_L = \frac{(E_r/E_m) - 1}{(E_r/E_m) + \xi_L} \tag{7}$$

$$\eta_w = \frac{(E_r/E_m) - 1}{(E_r/E_m) + \xi_w} \tag{8}$$

ξ_L and ξ_w are parameters dependent on the geometry of fillers expressed as (Van 2001)

$$\xi_L = \frac{2L}{3t} \tag{9}$$

$$\xi_w = \frac{2W}{3t} \tag{10}$$

where L, W and t are the length, width, and thickness of rectangular fillers (rGOs). V_r is the volume fraction of fillers (rGOs) defined as follows

$$V_r = \frac{\Lambda_{rGO}}{\Lambda_{rGO} + (\rho_{rGO}/\rho_m)(1 - \Lambda_{rGO})} \tag{11}$$

in which Λ_{rGO} is the weight fraction of rGOs. Also, ρ_{rGO} and ρ_m are the mass density of rGOs and matrix, respectively. The variations of elastic modulus versus E_r/E_m, L/t, and V_r for various filler geometry factors are depicted in Fig. 2.

According to the rule of mixture, the mass density and Poisson's ratio of rGORC plate are expressed as

$$\rho = \rho_{rGO} V_r + \rho_m (1 - V_r) \tag{12}$$

$$\nu = \nu_{rGO} V_r + \nu_m (1 - V_r) \tag{13}$$

in the above equations, ν_{rGO} and ν_m refer to the Poisson's ratio of rGOs and matrix, respectively. In this research, uniform and functionally graded distribution types of rGOs are assumed as follows

$$V_r(z) = V_r \qquad \text{(UD)} \tag{14}$$

$$V_r(z) = 2V_r \left(\frac{h-2|z|}{h}\right) \qquad \text{(FG-O)} \tag{15}$$

$$V_r(z) = 4V_r \left(\frac{|z|}{h}\right) \qquad \text{(FG-X)} \tag{16}$$

$$V_r(z) = V_r \left(\frac{h+2z}{h}\right) \qquad \text{(FG-V)} \tag{17}$$

3. Refined plate theory (RPT)

Based on refined plate theory (RPT), the displacement field can be written as

$$\begin{aligned} u(x,y,z) &= u_0 - z\frac{\partial w_b}{\partial x} + g(z)\frac{\partial w_s}{\partial x} \\ v(x,y,z) &= v_0 - z\frac{\partial w_b}{\partial y} + g(z)\frac{\partial w_s}{\partial y} \\ w(x,y,z) &= w_b + w_s \end{aligned} \tag{18}$$

where u, v, w are displacements in the x, y, z directions, u_0, v_0, w_b and w_s are mid-plane bending and shear deflections. Also, the function $g(z)$ stands for the distribution of transverse shear strains and stresses through plate thickness. Also, the transverse normal strain is assumed $\varepsilon_{zz} = 0$. There are other shear deformation theories, which can be used for the analysis of plates (Carrera *et al*. 2015, 2017). In this research, Reddy's third-order function is selected for $g(z)$ as follows (Reddy 1984)

$$g(z) = -\frac{4}{3}\left(\frac{z^3}{h^2}\right) \tag{19}$$

The relationships between strains and displacements can be expressed as

$$\{\varepsilon\} = \begin{Bmatrix} \varepsilon_x \\ \varepsilon_y \\ \gamma_{xy} \end{Bmatrix} = \begin{Bmatrix} \varepsilon_x^0 \\ \varepsilon_y^0 \\ \gamma_{xy}^0 \end{Bmatrix} + z \begin{Bmatrix} k_x^b \\ k_y^b \\ k_{xy}^b \end{Bmatrix} + g \begin{Bmatrix} k_x^s \\ k_y^s \\ k_{xy}^s \end{Bmatrix} \tag{20}$$

$$\{\gamma\} = \begin{Bmatrix} \gamma_{xz} \\ \gamma_{yz} \end{Bmatrix} = (1 + g') \begin{Bmatrix} \gamma_{xz}^s \\ \gamma_{yz}^s \end{Bmatrix} \tag{21}$$

where

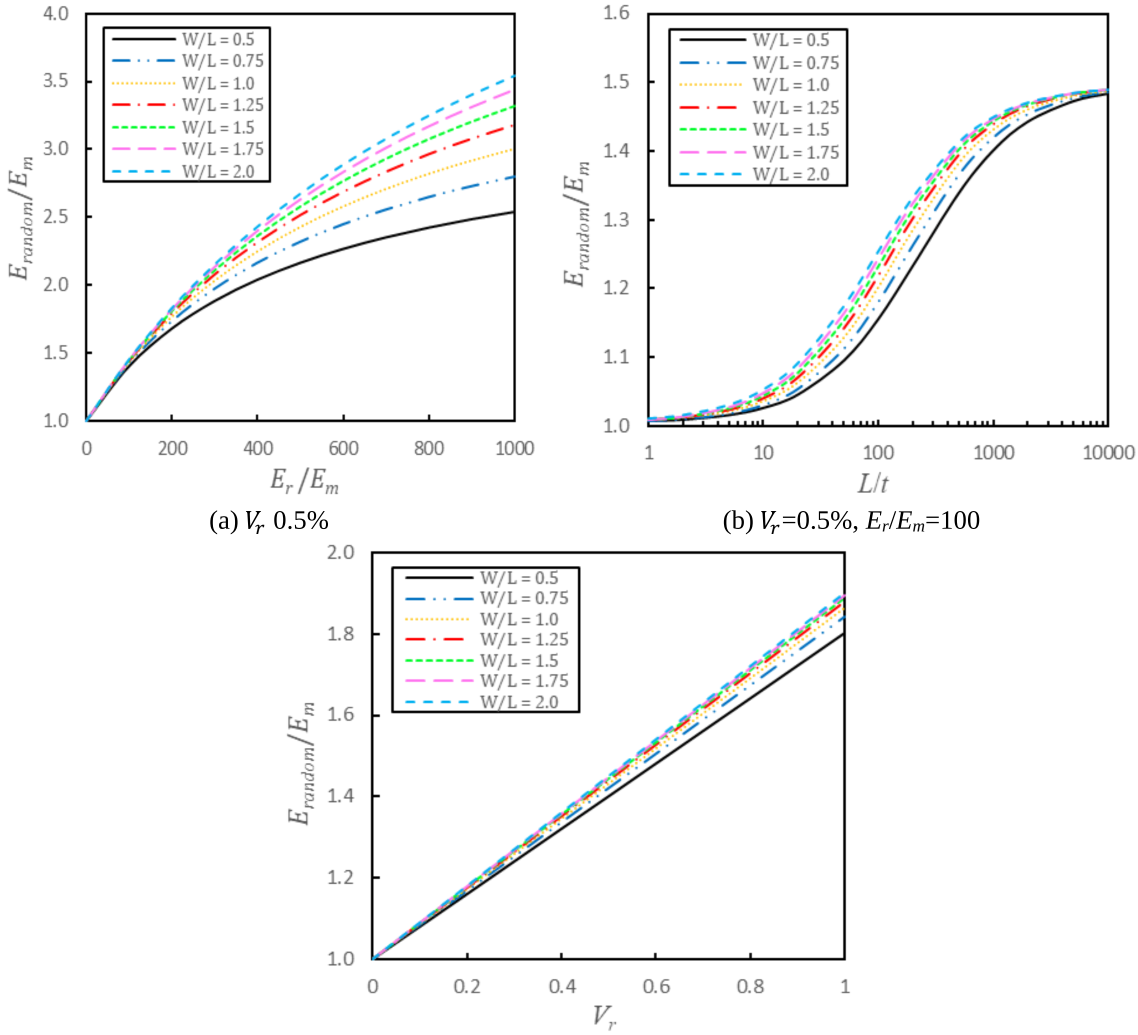

(a) V_r 0.5%

(b) V_r=0.5%, E_r/E_m=100

(c) E_r/E_m=100, L/t=1000

Fig. 2 Variations of elastic modulus for various filler geometry factors

$$\begin{Bmatrix} \varepsilon_x^0 \\ \varepsilon_y^0 \\ \gamma_{xy}^0 \end{Bmatrix} = \begin{Bmatrix} \dfrac{\partial u_0}{\partial x} \\ \dfrac{\partial v_0}{\partial y} \\ \dfrac{\partial u_0}{\partial y} + \dfrac{\partial v_0}{\partial x} \end{Bmatrix}, \begin{Bmatrix} k_x^b \\ k_y^b \\ k_{xy}^b \end{Bmatrix} = -\begin{Bmatrix} \dfrac{\partial^2 w_b}{\partial x^2} \\ \dfrac{\partial^2 w_b}{\partial y^2} \\ 2\dfrac{\partial^2 w_b}{\partial x \partial y} \end{Bmatrix}, \begin{Bmatrix} k_x^s \\ k_y^s \\ k_{xy}^s \end{Bmatrix} = \begin{Bmatrix} \dfrac{\partial^2 w_s}{\partial x^2} \\ \dfrac{\partial^2 w_s}{\partial y^2} \\ 2\dfrac{\partial^2 w_s}{\partial x \partial y} \end{Bmatrix}, \begin{Bmatrix} \gamma_{xz}^s \\ \gamma_{yz}^s \end{Bmatrix} = \begin{bmatrix} \dfrac{\partial w_s}{\partial x} \\ \dfrac{\partial w_s}{\partial y} \end{bmatrix} \tag{22}$$

Also, the relationships between curvatures and displacements can be written as

$$\{\chi_1\} = \begin{Bmatrix} \chi_x \\ \chi_y \\ \chi_{xy} \end{Bmatrix} = \begin{Bmatrix} \chi_x^b \\ \chi_y^b \\ \chi_{xy}^b \end{Bmatrix} + (1 - g') \begin{Bmatrix} \chi_x^s \\ \chi_y^s \\ \chi_{xy}^s \end{Bmatrix} \tag{23}$$

$$\{\chi_2\} = \begin{Bmatrix} \chi_{xz} \\ \chi_{yz} \end{Bmatrix} = \begin{Bmatrix} \chi_{xz}^0 \\ \chi_{yz}^0 \end{Bmatrix} + g'' \begin{Bmatrix} \chi_{xz}^1 \\ \chi_{yz}^1 \end{Bmatrix} \tag{24}$$

$$\chi_z = 0 \tag{25}$$

where

$$\begin{Bmatrix} \chi_x^b \\ \chi_y^b \\ \chi_{xy}^b \end{Bmatrix} = \begin{Bmatrix} \dfrac{\partial^2 w_b}{\partial x \partial y} \\ -\dfrac{\partial^2 w_b}{\partial x \partial y} \\ \dfrac{1}{2}\left(\dfrac{\partial^2 w_b}{\partial y^2} - \dfrac{\partial^2 w_b}{\partial x^2}\right) \end{Bmatrix}, \begin{Bmatrix} \chi_x^s \\ \chi_y^s \\ \chi_{xy}^s \end{Bmatrix} = \begin{Bmatrix} \dfrac{1}{2}\dfrac{\partial^2 w_s}{\partial x \partial y} \\ -\dfrac{1}{2}\dfrac{\partial^2 w_s}{\partial x \partial y} \\ \dfrac{1}{4}\left(\dfrac{\partial^2 w_s}{\partial y^2} - \dfrac{\partial^2 w_s}{\partial x^2}\right) \end{Bmatrix} \tag{26}$$

$$\begin{Bmatrix} \chi_{xz}^0 \\ \chi_{yz}^0 \end{Bmatrix} = \frac{1}{4} \begin{Bmatrix} (\dfrac{\partial^2 v_0}{\partial x^2} - \dfrac{\partial^2 u_0}{\partial y \partial x}) \\ (\dfrac{\partial^2 v_0}{\partial y \partial x} - \dfrac{\partial^2 u_0}{\partial y^2}) \end{Bmatrix}, \begin{Bmatrix} \chi_{xz}^1 \\ \chi_{yz}^1 \end{Bmatrix} = \frac{1}{4} \begin{Bmatrix} -\dfrac{\partial w_s}{\partial y} \\ \dfrac{\partial w_s}{\partial x} \end{Bmatrix} \tag{27}$$

By substituting Eqs. (20)-(27) into Eq. (1) the stress resultants can be obtained as

$$\begin{Bmatrix} \{N\} \\ \{M^b\} \\ \{M^s\} \end{Bmatrix} = \mathrm{D^b} \begin{Bmatrix} \{\varepsilon^0\} \\ \{k^b\} \\ \{k^s\} \end{Bmatrix} \tag{28}$$

$$\{S^s\} = \mathrm{D^s}\{\gamma^s\} \tag{29}$$

$$\begin{Bmatrix} \{A^\chi\} \\ \{B^\chi\} \end{Bmatrix} = \mathrm{D}_\chi^\mathrm{b} \begin{Bmatrix} \{\chi^b\} \\ \{\chi^s\} \end{Bmatrix} \tag{30}$$

$$\begin{Bmatrix} \{D^\chi\} \\ \{E^\chi\} \end{Bmatrix} = \mathrm{D}_\chi^\mathrm{s} \begin{Bmatrix} \{\chi^0\} \\ \{\chi^1\} \end{Bmatrix} \tag{31}$$

The material matrices can be given as follows

$$\mathrm{D^b} = \begin{bmatrix} A & B & D \\ B & C & E \\ D & E & F \end{bmatrix} \tag{32}$$

$$(A,B,C,D,E,F) = \int_{-h/2}^{h/2} \begin{bmatrix} 1 & \nu & 0 \\ \nu & 1 & 0 \\ 0 & 0 & \dfrac{1-\nu}{2} \end{bmatrix} \frac{E}{1-\nu^2}(1,z,z^2,g,zg,g^2)dz \tag{33}$$

$$\mathrm{D^s} = \begin{bmatrix} 1 & 0 \\ 0 & 1 \end{bmatrix} \int_{-h/2}^{h/2} \frac{E(1+g')^2}{2(1+\nu)} dz \tag{34}$$

$$\mathrm{D}_\chi^\mathrm{b} = \begin{bmatrix} A_\chi & B_\chi \\ B_\chi & C_\chi \end{bmatrix} \tag{35}$$

$$(A_\chi, B_\chi, C_\chi) = \begin{bmatrix} 1 & 0 & 0 \\ 0 & 1 & 0 \\ 0 & 0 & 2 \end{bmatrix} \int_{-h/2}^{h/2} (1, (1-g'), (1-g')^2) \frac{E}{(1+\nu)} l^2 dz \tag{36}$$

$$\mathrm{D}_\chi^{\mathrm{s}} = \begin{bmatrix} G_\chi & H_\chi \\ H_\chi & I_\chi \end{bmatrix} \tag{37}$$

$$(G_\chi, H_\chi, I_\chi) = \begin{bmatrix} 2 & 0 \\ 0 & 2 \end{bmatrix} \int_{-h/2}^{h/2} (1, g'', (g'')^2) \frac{E}{(1+\nu)} l^2 \, dz \tag{38}$$

The kinetic energy is expressed as

$$T = \frac{1}{2} \int \rho \, [(\dot{u})^2 + (\dot{v})^2 + (\dot{w})^2] dV \tag{39}$$

The variation of the kinetic energy is given as

$$\delta T = \iint (\dot{u}\delta\dot{u} + \dot{v}\delta\dot{v} + w\delta\dot{w}) \, \rho dz dA = -\int \delta\tilde{u}^T m \ddot{\tilde{u}} dV \tag{40}$$

where m stands for the mass matrix defined as follows

$$m = \begin{bmatrix} I_0 & 0 & 0 \\ 0 & I_0 & 0 \\ 0 & 0 & I_* \end{bmatrix}, I_0 = \begin{bmatrix} I_1 & I_2 & I_4 \\ I_2 & I_3 & I_5 \\ I_4 & I_5 & I_6 \end{bmatrix}, I_* = \begin{bmatrix} I_1 & I_7 & 0 \\ I_7 & I_8 & 0 \\ 0 & 0 & 0 \end{bmatrix} \tag{41}$$

$$(I_1, I_2, I_3, I_4, I_5, I_6, I_7, I_8) = \int_{-h/2}^{h/2} (1, z, z^2, g, zg, g^2, (1+g'), (1+g')^2) \, \rho dz \tag{42}$$

$$\tilde{u} = \{u_0, -\frac{\partial w_b}{\partial x}, \frac{\partial w_s}{\partial x}, v_0, -\frac{\partial w_b}{\partial y}, \frac{\partial w_s}{\partial y}, (w_b + w_s), 0, 0\}^T \tag{43}$$

The variation of the work done for buckling load can be expressed as follows

$$\delta W = \int \nabla^T \delta w \mathrm{P} \nabla w d\Omega \tag{44}$$

where

$$\mathrm{P} = \begin{bmatrix} N_x & N_{xy} \\ N_{xy} & N_y \end{bmatrix}, \nabla = [\frac{\partial}{\partial x} \;\; \frac{\partial}{\partial y}]^T \tag{45}$$

4. A brief introduction of NURBS basis functions

4.1 NURBS basis functions

B-spline basis functions with degree *p* can be expressed as (Hughes *et al*. 2005)

$$N_{i,0}(u)=\begin{cases}1 & if\ u_i\le u\le u_{i+1}\\ 0 & otherwise\end{cases}$$
$$N_{i,p}(u)=\frac{u-u_i}{u_{i+p}-u_i}N_{i,p-1}(u)+\frac{u_{i+p+1-u}}{u_{i+p+1}-u_{i+1}}N_{i+1,p-1}(u) \tag{46}$$

A piecewise-polynomial B-spline surface of degree *p* is defined as

$$S(u,v)=\sum_{i=0}^{n}\sum_{j=0}^{m}N_{i,p}(u)N_{j,q}(v)P_{i,j} \tag{47}$$

where $P_{i,j}$ form a bidirectional control net, $N_{i,p}(u)$ and $N_{j,q}(v)$ are the B-spline basis functions. Also, the NURBS surface of degree *p* can be written as follows

$$S_{i,j}(u,v)=\frac{\sum_{i=0}^{n}\sum_{j=0}^{m}N_{i,p}(u)\,N_{j,q}\,(v)w_{i,j}P_{i,j}}{\sum_{i=0}^{n}\sum_{j=0}^{m}N_{i,p}(u)\,N_{j,q}\,(v)w_{i,j}} \tag{48}$$

where $w_{i,j}$ are the weights.

4.2 RPT formulation based on NURBS approximations

The equation of free vibration can be derived by using Hamilton's principle as

$$\delta\int_0^t(T-U)dt=\int_0^t(\delta T-\delta U)dt=0\Rightarrow\int\delta\varepsilon^T\mathrm{D}\varepsilon+\delta\chi^T\mathrm{D}_\chi\chi dV=-\int\delta\,\tilde{u}^Tm\ddot{\tilde{u}}dV \tag{49}$$

By simplifying Eq. (49), one can have the below equation.

$$(\mathrm{K}-\omega^2\mathrm{M})\mathrm{D}=0 \tag{50}$$

where

$$\mathrm{M}=\int\tilde{R}^Tm\tilde{R}d\Omega \tag{51}$$

$$\tilde{R}=\begin{bmatrix}R_i & 0 & 0 & 0 & 0 & 0 & 0 & 0 & 0\\ 0 & 0 & 0 & R_i & 0 & 0 & 0 & 0 & 0\\ 0 & -R_{i,x} & 0 & 0 & -R_{i,y} & 0 & R_i & 0 & 0\\ 0 & 0 & R_{i,x} & 0 & 0 & R_{i,y} & R_i & 0 & 0\end{bmatrix}^T \tag{52}$$

and the global stiffness matrix K can be expressed as follows

$$\mathrm{K}=\int(\mathrm{B^m}^{\mathrm{T}}\mathrm{D^b}\mathrm{B^m}+\mathrm{B^s}^{\mathrm{T}}\mathrm{D^s}\mathrm{B^s}+\mathrm{B}_\chi^{\mathrm{m}\,\mathrm{T}}\mathrm{D}_\chi^{\mathrm{m}}\mathrm{B}_\chi^{\mathrm{m}}+\mathrm{B}_\chi^{\mathrm{s}\,\mathrm{T}}\mathrm{D}_\chi^{\mathrm{s}}\mathrm{B}_\chi^{\mathrm{s}})d\Omega \tag{53}$$

where

$$\mathrm{B^m}=\begin{bmatrix}R_{i,x} & 0 & R_{i,y} & 0 & 0 & 0 & 0 & 0 & 0\\ 0 & R_{i,y} & R_{i,x} & 0 & 0 & 0 & 0 & 0 & 0\\ 0 & 0 & 0 & -R_{i,xx} & -R_{i,yy} & -2R_{i,xy} & 0 & 0 & 0\\ 0 & 0 & 0 & 0 & 0 & 0 & R_{i,xx} & R_{i,yy} & 2R_{i,xy}\end{bmatrix}^T \tag{54}$$

$$\mathrm{B^s}=\begin{bmatrix}0 & 0 & 0 & R_{i,x}\\ 0 & 0 & 0 & R_{i,y}\end{bmatrix} \tag{55}$$

$$\mathrm{B_\chi^m}=\frac{1}{4}\begin{bmatrix}0 & 0 & 0 & 0 & 0 & 0\\ 0 & 0 & 0 & 0 & 0 & 0\\ 4R_{i,xy} & -4R_{i,xy} & 2(R_{i,yy}-R_{i,xx}) & 0 & 0 & 0\\ 0 & 0 & 0 & 2R_{i,xy} & -2R_{i,xy} & (R_{i,yy}-R_{i,xx})\end{bmatrix}^T \tag{56}$$

$$\mathrm{B_\chi^s}=\frac{1}{4}\begin{bmatrix}-R_{i,xy} & R_{i,xx} & 0 & 0\\ -R_{i,yy} & R_{i,xy} & 0 & 0\\ 0 & 0 & 0 & -R_{i,y}\\ 0 & 0 & 0 & R_{i,x}\end{bmatrix} \tag{57}$$

Similarly, one can derive the weak form of the total energy for buckling analysis as follows

$$\delta\Pi=0 \;\Rightarrow\; \int \delta\varepsilon^T \mathrm{D}\varepsilon+\delta\chi^T \mathrm{D_c}\chi dV=\int \nabla^{\mathrm{T}}\delta w \mathrm{P}\nabla w d\Omega \tag{58}$$

By simplifying the above equation, one can have the simplified equation for buckling analysis as

$$\left(\mathrm{K}-\lambda_{\mathrm{cr}}\mathrm{K_g}\right)\mathrm{D}=0 \tag{59}$$

where λ_{cr} is the critical load. The geometric stiffness matrix $\mathrm{K_g}$ can be written as

$$\mathrm{K_g}=\int (\mathrm{B^{g^T}PB^g})d\Omega \tag{60}$$

$$\mathrm{B^g}=\begin{bmatrix}0 & 0 & R_{i,x} & R_{i,x}\\ 0 & 0 & R_{i,y} & R_{i,y}\end{bmatrix} \tag{61}$$

5. Results and discussion

In this section, IGA results are provided for the free vibration, and buckling of functionally graded reduced graphene oxide reinforced nanocomposite (FG rGORC) plates. The material length scale parameter *l* is assumed to be constant and selected as 17.6 μm (Lam *et al*. 2003, Liu *et al*. 2017). The material properties and geometric parameters of rGOs are assumed as E_{rGO} = 250 GPa, (Gómez-Navarro *et al*. 2008, Li *et al*. 2015, Iqbal *et al*. 2016, Suk *et al*. 2010), ρ_{rGO} = 2250 kg/m^3 (Li *et al*. 2015), ν_{rGO} = 0.165 (Suk *et al*. 2010), $L_{rGO}=W_{rGO}$ = 1 μm (Gómez-Navarro *et al*. 2008, Li *et al*. 2015), t_{rGO} = 1 nm (Li *et al*. 2015). Besides, epoxy is considered as a polymer matrix having material properties E_m = 3 GPa, ρ_m = 1200 kg/m^3, ν_m = 0.34 (Zhang *et al*. 2018). The dimensionless fundamental frequency $\bar{\omega}=\omega h\sqrt{\rho_m/E_m}$ and critical biaxial buckling load $\bar{P}=P_{cr}a^2/h^3E_m$ are considered for all problems, unless otherwise clearly expressed. Also, the details of simply supported (SSSS) and clamped (CCCC) boundary conditions for square plates are assumed as follows:

SSSS:

$$v_0=w_b=w_s=0 \text{ at } \mathrm{x}=0,a$$

CCCC:

$$u_0 = w_b = w_s = 0 \text{ at } y = 0, b$$

$$u_0 = v_0 = w_b = w_s = 0$$

5.1 Convergence study

As the first example, the dimensionless natural frequencies $\bar{\omega} = \omega a^2\sqrt{\rho h/D}$ of isotropic plates are tabulated in Table 1 for length to thickness ratio *a/h* = 10 ($D = Eh^3/12(1-\nu^2)$). It is assumed that $E = 70$ GPa, $\rho = 2702 \text{ kg/m}^3$, $\nu = 0.3$. The results are given for different meshes and degrees *p*=2, 3, 4. As it can be seen, the obtained IGA results converge so fast, particularly for quartic NURBS elements (*p*=4) and simply boundary conditions (SSSS). Also, the obtained results are very close to solutions obtained based on first-order shear deformation theory FSDT (Zhao *et al*. 2019). For the following problems, a mesh of 11×11 quartic NURBS elements (*p*=4) can be sufficient and selected as illustrated in Fig. 3.

Table 1 Convergence of the dimensionless natural frequencies $\bar{\omega} = \omega a^2\sqrt{\rho h/D}$ of isotropic plates

B.S.	Mode	*p*	Mesh					Zhao *et al.* (2019)
			3×3	5×5	7×7	9×9	11×11	
SSSS	1	2	19.5148	19.2184	19.1423	19.1116	19.0962	19.065
		3	19.0745	19.0664	19.0656	19.0654	19.0653	
		4	19.0655	19.0653	19.0653	19.0653	19.0653	
	2	2	51.1442	47.3293	46.3955	46.0290	45.8473	45.482
		3	45.9212	45.5462	45.5007	45.4917	45.4890	
		4	45.6280	45.4895	45.4872	45.4870	45.4870	
CCCC	1	2	43.3860	35.9848	34.4729	33.8809	33.5821	32.525
		3	33.4530	33.1498	33.0613	33.0187	32.9935	
		4	33.1191	33.0343	32.9922	32.9693	32.9552	
	2	2	123.6352	75.2157	69.0208	66.8325	65.7757	62.042
		3	66.0662	64.3434	63.9842	63.8490	63.7754	
		4	64.6997	63.9005	63.7708	63.7067	63.6687	

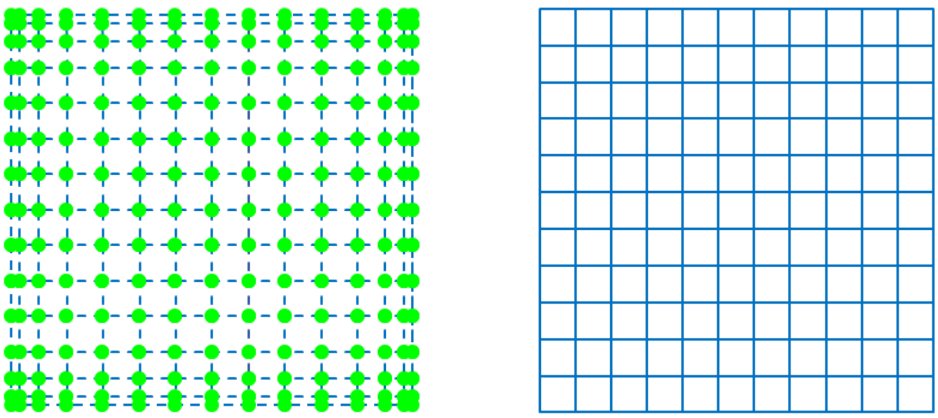

(a) Control points (b) Elements

Fig. 3 Meshing of 11×11 quartic elements

Table 2 Dimensionless fundamental frequency $\bar{\omega} = \omega h\sqrt{\rho_m/E_m}$ of GPLRC plates (Λ=1%, $\xi_L = 2L/t, \xi_w = 2W/t$)

B.C.	Type	Model	*l/h*					
			0	0.2	0.4	0.6	0.8	1
SSSS	Pure epoxy	Thai *et al*. (2019a)	0.0584	0.0631	0.0753	0.0922	0.1116	0.1324
		Present	0.0584	0.0631	0.0753	0.0922	0.1116	0.1324
	UD	Thai *et al*. (2019a)	0.1216	0.1313	0.1568	0.1919	0.2323	0.2757
		Present	0.1216	0.1313	0.1568	0.1919	0.2323	0.2757
CCCC	Pure epoxy	Thai *et al*. (2019a)	0.0999	0.1087	0.1314	0.1622	0.1974	0.2350
		Present	0.1007	0.1095	0.1322	0.1630	0.1982	0.2358
	UD	Thai *et al*. (2019a)	0.2078	0.2261	0.2735	0.3378	0.4111	0.4111
		Present	0.2096	0.2278	0.2751	0.3394	0.4127	0.4911

Table 3 Dimensionless natural frequencies $\bar{\omega} = \omega h\sqrt{\rho_m/E_m}$ of FG rGORC plates (*l/h*=0, Λ_{rGO}=1%)

B.C.	Type	*b/a*	Mode 1			Mode 2		
			a/h=5	*a/h*=10	*a/h*=20	*a/h*=5	*a/h*=10	*a/h*=20
SSSS	UD	0.5	0.4521	0.1638	0.0436	0.5469	0.2260	0.0688
		1.0	0.2510	0.0688	0.0177	0.4521	0.1638	0.0436
		1.5	0.1871	0.0502	0.0128	0.3014	0.0943	0.0244
	FG-O	0.5	0.4521	0.1537	0.0405	0.5242	0.2261	0.0641
		1.0	0.2369	0.0641	0.0164	0.4521	0.1537	0.0405
		1.5	0.1758	0.0467	0.0119	0.3014	0.0880	0.0227
	FG-X	0.5	0.4521	0.1723	0.0463	0.5619	0.2261	0.0730
		1.0	0.2624	0.0730	0.0188	0.4521	0.1723	0.0463
		1.5	0.1965	0.0533	0.0136	0.3014	0.0998	0.0260
	FG-V	0.5	0.4521	0.1618	0.0430	0.5415	0.2261	0.0679
		1.0	0.2481	0.0679	0.0174	0.4521	0.1618	0.0430
		1.5	0.1848	0.0495	0.0126	0.3014	0.0931	0.0241
CCCC	UD	0.5	0.7939	0.2822	0.0828	1.0040	0.3604	0.1067
		1.0	0.3894	0.1186	0.0317	0.6973	0.2286	0.0635
		1.5	0.3073	0.0907	0.0239	0.4520	0.1374	0.0367
	FG-O	0.5	0.7872	0.2709	0.0777	0.9954	0.3462	0.1001
		1.0	0.3763	0.1116	0.0295	0.6814	0.2168	0.0593
		1.5	0.2953	0.0851	0.0223	0.4361	0.1293	0.0342
	FG-X	0.5	0.7886	0.2894	0.0871	0.9972	0.3695	0.1122
		1.0	0.3967	0.1243	0.0337	0.7023	0.2376	0.0673
		1.5	0.3149	0.0954	0.0254	0.4611	0.1442	0.0390
	FG-V	0.5	0.7899	0.2796	0.0818	0.9988	0.3571	0.1054
		1.0	0.3862	0.1172	0.0313	0.6923	0.2262	0.0628
		1.5	0.3045	0.0896	0.0236	0.4480	0.1358	0.0363

5.2 Free vibration analysis

The results of the dimensionless fundamental frequency $\bar{\omega} = \omega h\sqrt{\rho_m/E_m}$ of graphene platelet reinforced nanocomposite (GPLRC) plates are tabulated in Table 2 for *l/h* = 0, 0.2, 0.4, 0.6, 0.8, 1, Λ = 1%, $\xi_L = 2L/t$, and $\xi_w = 2W/t$. The material properties are assumed as E_{GPL} = 1010 GPa, L_{GPL} = 2.5 μm, W_{GPL} = 1.5 μm, t_{GPL} = 1.5 nm, ρ_{GPL} = 1060 kg/m^3, $\nu_{GPL} = 0.186$, E_m = 3 GPa, ρ_m=120t kg/m^3, and ν_m =0.34 (Thai *et al*. 2019a). The UD type and pure epoxy matrix are considered. As observed, the present results are very close to those of higher-order shear deformation theory (HSDT) (Thai *et al*. 2019a), particularly for the SSSS boundary condition.

Table 3 gives the dimensionless natural frequencies of FG rGORC plates by assuming *l/h*=0 and Λ_{rGO}=1%. The increase of *a/h* and *b/a* results in the decrease of natural frequencies. Also, FG-X and FG-O give the largest and lowest values for natural frequencies, respectively.

In Tables 4 and 5, the results are given for the dimensionless fundamental frequency of FG rGORC plates with SSSS and CCCC boundary conditions. As can be seen, the increase of *h/l* and Λ_{rGO} remarkably leads to the decrease and increase of fundamental frequency, respectively. For example, adding only 1% weight fraction of rGO by assuming FG-X and UD types leads to the fundamental frequency of about 23% and 18% higher than that of the epoxy plate, respectively. The percentage of frequency change $\omega_{\mathrm{rGORC}}/\omega_{\mathrm{epoxy}}$ (%) versus weight fraction Λ_{rGO} for various FG distribution types is depicted in Fig. 4(a). There can be found a nearly linear relationship between

Table 4 Dimensionless fundamental frequency $\bar{\omega} = \omega h\sqrt{\rho_m/E_m}$ of FG rGORC plates (SSSS)

Type	Λ_{rGO}(%)	*h/l*				
		∞	10	5	2	1
Pure epoxy	0.0	0.0584	0.0596	0.0631	0.0833	0.1324
UD	0.2	0.0606	0.0619	0.0655	0.0865	0.1374
	0.4	0.0628	0.0641	0.0678	0.0895	0.1422
	0.6	0.0648	0.0662	0.0700	0.0925	0.1469
	0.8	0.0668	0.0682	0.0722	0.0954	0.1515
	1.0	0.0688	0.0702	0.0743	0.0981	0.1559
FG-O	0.2	0.0596	0.0609	0.0645	0.0857	0.1368
	0.4	0.0608	0.0621	0.0659	0.0881	0.1412
	0.6	0.0619	0.0633	0.0673	0.0903	0.1454
	0.8	0.0630	0.0645	0.0686	0.0926	0.1495
	1.0	0.0641	0.0656	0.0699	0.0947	0.1535
FG-X	0.2	0.0616	0.0629	0.0664	0.0872	0.1379
	0.4	0.0647	0.0659	0.0696	0.0910	0.1433
	0.6	0.0676	0.0688	0.0726	0.0946	0.1484
	0.8	0.0703	0.0716	0.0755	0.0981	0.1534
	1.0	0.0730	0.0743	0.0782	0.1014	0.1582
FG-V	0.2	0.0606	0.0618	0.0654	0.0865	0.1374
	0.4	0.0626	0.0639	0.0676	0.0894	0.1421
	0.6	0.0645	0.0658	0.0697	0.0922	0.1467
	0.8	0.0662	0.0676	0.0716	0.0949	0.1512
	1.0	0.0679	0.0693	0.0734	0.0975	0.1555

Table 5 Dimensionless fundamental frequency $\bar{\omega} = \omega h\sqrt{\rho_m/E_m}$ of FG rGORC plates (CCCC)

Type	Λ_{rGO}(%)	*h/l*				
		∞	10	5	2	1
Pure epoxy	0.0	0.1007	0.1030	0.1095	0.1468	0.2358
UD	0.2	0.1045	0.1069	0.1136	0.1524	0.2447
	0.4	0.1082	0.1106	0.1176	0.1578	0.2534
	0.6	0.1118	0.1143	0.1215	0.1630	0.2617
	0.8	0.1152	0.1178	0.1252	0.1680	0.2698
	1.0	0.1186	0.1212	0.1289	0.1729	0.2777
FG-O	0.2	0.1031	0.1054	0.1122	0.1511	0.2436
	0.4	0.1053	0.1078	0.1148	0.1553	0.2513
	0.6	0.1075	0.1100	0.1174	0.1594	0.2586
	0.8	0.1096	0.1122	0.1199	0.1634	0.2658
	1.0	0.1116	0.1144	0.1223	0.1673	0.2728
FG-X	0.2	0.1059	0.1083	0.1150	0.1536	0.2458
	0.4	0.1109	0.1133	0.1202	0.1602	0.2554
	0.6	0.1155	0.1180	0.1252	0.1664	0.2647
	0.8	0.1200	0.1226	0.1300	0.1724	0.2737
	1.0	0.1243	0.1270	0.1346	0.1783	0.2824
FG-V	0.2	0.1045	0.1068	0.1135	0.1523	0.2447
	0.4	0.1079	0.1104	0.1174	0.1576	0.2532
	0.6	0.1112	0.1137	0.1209	0.1625	0.2614
	0.8	0.1143	0.1169	0.1244	0.1673	0.2693
	1.0	0.1172	0.1199	0.1276	0.1719	0.2770

frequency change (%) and weight fraction Λ_{rGO}. The effects of ratio *h/l* on the fundamental frequency of FG rGORC plates are also shown in Figs. 4 (b) and (c) for various distribution types and weight fraction Λ_{rGO}.

Fig. 5 depicts the effect of *L/t* on the fundamental frequency of FG rGORC plates. It is assumed that Λ_{rGO}=1%, *l/h*=0 and CCCC boundary condition. Similar to the deflection, for *L/t*<2000 the fundamental frequency remarkably changes. Furthermore, when *L/t* is beyond 2000, the fundamental frequency remains almost unchanged. In addition, square rGO platelets (*W/L*=1) give fundamental frequencies higher than those of rectangular rGO platelets (*W/L*=0.25).

5.3 Buckling analysis

To validate the IGA model for buckling analysis, the obtained results for the dimensionless biaxial buckling load $P = P_{cr}a^2/E_m h^3$ of graphene, platelet reinforced nanocomposite (GPLRC) plates are given in Table 6 and also compared with those of reference (Arefi *et al*. 2019). To solve this problem, it is assumed that l=15 μm, Λ=1%, $\xi_L = 2L/t, \xi_w = 2W/t$, by considering UD and SSSS boundary conditions. The material properties are also assumed as E_{GPL}=1010 GPa, L_{GPL}=2.5 μm, W_{GPL}=1.5 μm, t_{GPL}=1.5 nm, ρ_{GPL}=1062.5 kg/m^3, ν_{GPL} =0.186, E_m=3 GPa, ρ_m=1200 kg/m^3, and ν_m =0.34 (Arefi *et al*. 2019). Similar to the free vibration problems, the obtained IGA results for buckling analysis are close to reference (Arefi *et al*. 2019), particularly for thin plates.

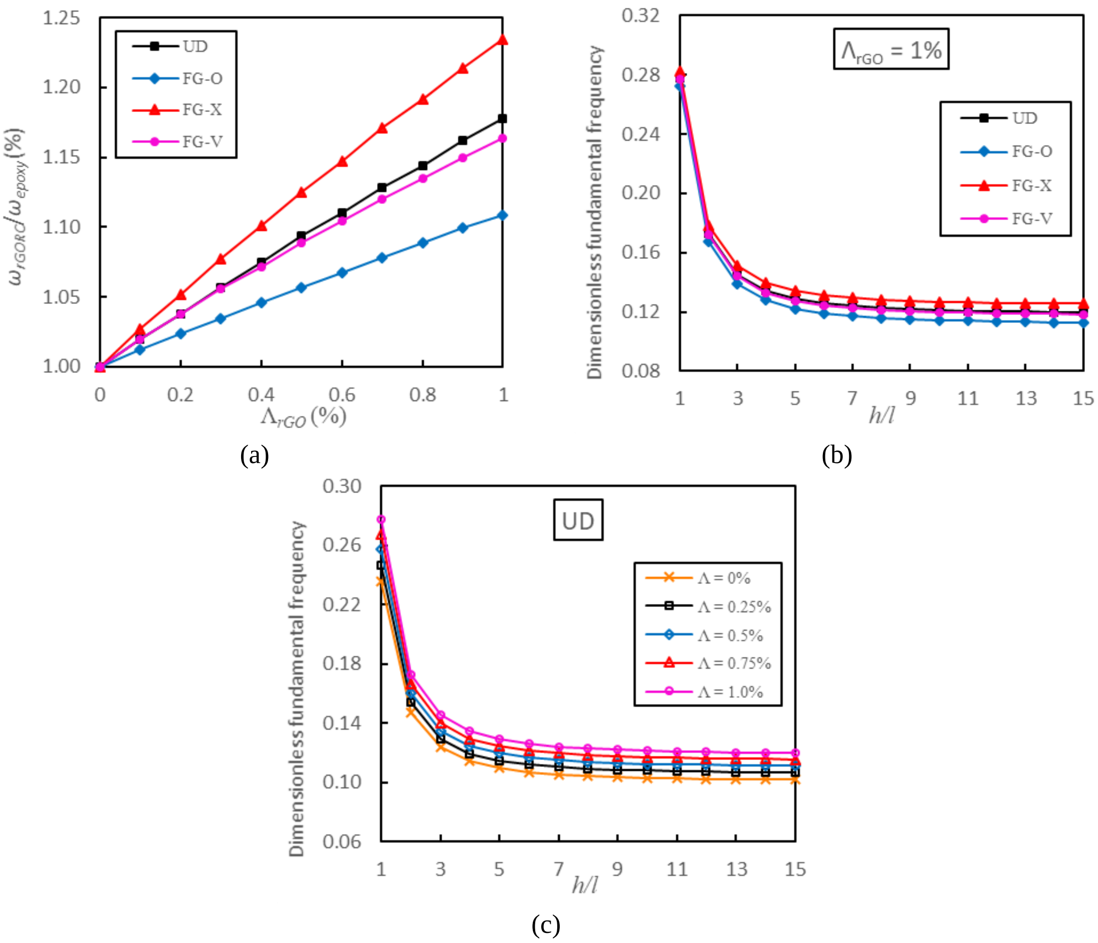

Fig. 4 Effect of rGO weight fraction on the fundamental frequency change (%) of FG rGORC plates for various distribution types (CCCC)

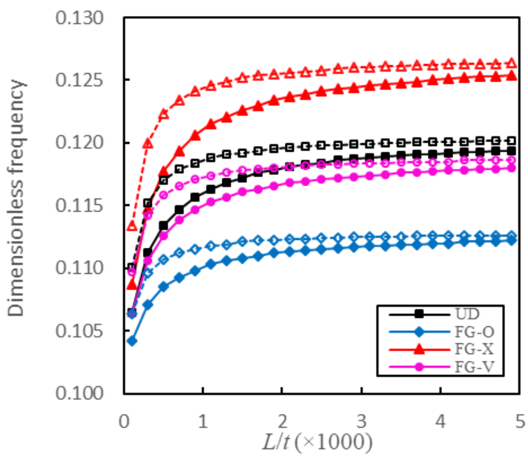

Fig. 5 Effect of L/t ratio on the dimensionless fundamental frequency of FG rGORC plates for various distribution types (Solid line: W/L=0.25, dashed line: W/L=1, Λ_{rGO}=1%, l/h=0, CCCC)

Table 6 Dimensionless biaxial buckling load $P = P_{cr}a^2/E_m h^3$ of GPLRC plates (l=15 μm, Λ=1%, $\xi_L = 2L/t, \xi_w = 2W/t$, UD, SSSS)

a/h	*h/l*	*b/a* = 0.5		*b/a* = 1	
		Arefi *et al*. (2019)	Present	Arefi *et al*. (2019)	Present
5	∞	12.6152	12.6008	6.4860	6.4833
	10	13.3060	13.2898	6.7873	6.7844
	5	15.3782	15.3564	7.6911	7.6873
	1	81.5841	81.3868	36.4996	36.4672
10	∞	17.4692	17.4650	7.5752	7.5745
	10	18.2395	18.2348	7.8898	7.8891
	5	20.5491	20.5432	8.8335	8.8325
	1	94.1970	94.1464	38.9666	38.9586
20	∞	19.3454	19.3443	7.9084	7.9082
	10	20.1358	20.1347	8.2260	8.2259
	5	22.5067	22.5053	9.1790	9.1788
	1	98.2682	98.2557	39.6560	39.6540
50	∞	19.9464	19.9463	8.0070	8.0070
	10	20.7422	20.7420	8.3255	8.3255
	5	23.1292	23.1290	9.2811	9.2810
	1	99.4945	99.4926	39.8549	39.8546

Table 7 Dimensionless buckling load $P = P_{cr}a^2/E_m h^3$ of FG rGORC plates (l/h=0, Λ_{rGO}=1%)

B.C.	Type	*b/a*	*a/h*=5	*a/h*=10	*a/h*=20
SSSS	UD	0.5	4.0628	5.6328	6.2396
		1.0	2.0908	2.4432	2.5509
		1.5	1.5951	1.7925	1.8499
	FG-O	0.5	3.7730	4.9698	5.4003
		1.0	1.8689	2.1233	2.1983
		1.5	1.4124	1.5531	1.5929
	FG-X	0.5	4.2428	6.2243	7.0545
		1.0	2.2760	2.7484	2.8993
		1.5	1.7554	2.0240	2.1047
CCCC	UD	0.5	7.1688	13.8568	18.1873
		1.0	4.2150	5.9283	6.6041
		1.5	3.5818	4.7510	5.1757
	FG-O	0.5	7.0682	12.7191	15.9641
		1.0	3.9259	5.2378	5.7183
		1.5	3.2952	4.1743	4.4740
	FG-X	0.5	7.0614	14.6500	20.2189
		1.0	4.3882	6.5401	7.4628
		1.5	3.7776	5.2757	5.8606
	FG-V	0.5	7.1009	13.6049	17.7556
		1.0	4.1459	5.7925	6.4360
		1.5	3.5177	4.6388	5.0428

Table 7 gives the dimensionless biaxial buckling load of FG rGORC plates for *l/h*=0 and Λ_{rGO}=1%. The increase of aspect ratio *b/a* results in the decrease of dimensionless biaxial buckling load. Furthermore, FG-X and FG-O give the largest and lowest biaxial critical buckling load, respectively.

The results of the dimensionless biaxial buckling load of FG rGORC plates are tabulated in Table 8 for various distribution types, weight fraction Λ_{rGO} and ratio *h/l*. Similar to the free vibration analysis, the increase of *h/l* and weight fraction Λ_{rGO} significantly leads to the decrease and increase of critical buckling load, respectively. As an example, by assuming weight fraction Λ_{rGO}=1% as well as FG-X and UD types, the critical buckling load increases over 53% and 39%, respectively compared to the pure epoxy plate. The percentage of critical biaxial buckling load change $P_{\mathrm{rGORC}}/P_{\mathrm{epoxy}}$ (%) versus weight fraction Λ_{rGO} is shown in Fig. 6(a). As observed, there is a nearly linear relationship between critical biaxial buckling load change (%) and weight fraction Λ_{rGO}. In Fig. 6(b), the dimensionless biaxial buckling load versus ratio *h/l* is shown. Also, the effect of ratio *h/l* on the dimensionless biaxial buckling load of FG rGORC plates is depicted in Fig. 6(c).

The effect of ratio *L/t* on the biaxial buckling load of FG rGORC plates is shown in Fig. 7 by assuming Λ_{rGO}=1%, *l/h*=0 and CCCC boundary condition. Similar to the free vibration, when *L/t* is beyond 2000, the critical buckling load remains almost constant. Moreover, the critical buckling load of composite plates made of square rGO platelets (*W/L*=1) is higher than that of rectangular rGO platelets (*W/L*=0.25).

Table 8 Dimensionless biaxial buckling load $P = P_{cr}a^2/E_m h^3$ of FG rGORC plates (CCCC)

Type	Λ_{rGO}(%)	*h/l*				
		∞	10	5	2	1
Pure epoxy	0.0	4.2581	4.4464	5.0111	8.9567	23.0148
UD	0.2	4.5909	4.7940	5.4029	9.6578	24.8182
	0.4	4.9243	5.1422	5.7955	10.3605	26.6259
	0.6	5.2583	5.4910	6.1889	11.0647	28.4376
	0.8	5.5930	5.8406	6.5830	11.7704	30.2535
	1.0	5.9283	6.1908	6.9779	12.4776	32.0736
FG-O	0.2	4.4586	4.6604	5.2656	9.4989	24.6024
	0.4	4.6562	4.8717	5.5181	10.0419	26.1932
	0.6	4.8516	5.0809	5.7690	10.5857	27.7874
	0.8	5.0453	5.2887	6.0189	11.1304	29.3850
	1.0	5.2378	5.4954	6.2681	11.6760	30.9861
FG-X	0.2	4.7191	4.9238	5.5372	9.8162	25.0336
	0.4	5.1774	5.3987	6.0616	10.6770	27.0566
	0.6	5.6333	5.8715	6.5846	11.5393	29.0839
	0.8	6.0875	6.3428	7.1067	12.4030	31.1157
	1.0	6.5401	6.8128	7.6281	13.2684	33.1520
FG-V	0.2	4.5839	4.7870	5.3960	9.6507	24.8110
	0.4	4.8983	5.1162	5.7694	10.3339	26.5989
	0.6	5.2035	5.4361	6.1337	11.0085	28.3808
	0.8	5.5011	5.7486	6.4906	11.6763	30.1585
	1.0	5.7925	6.0547	6.8413	12.3386	31.9333

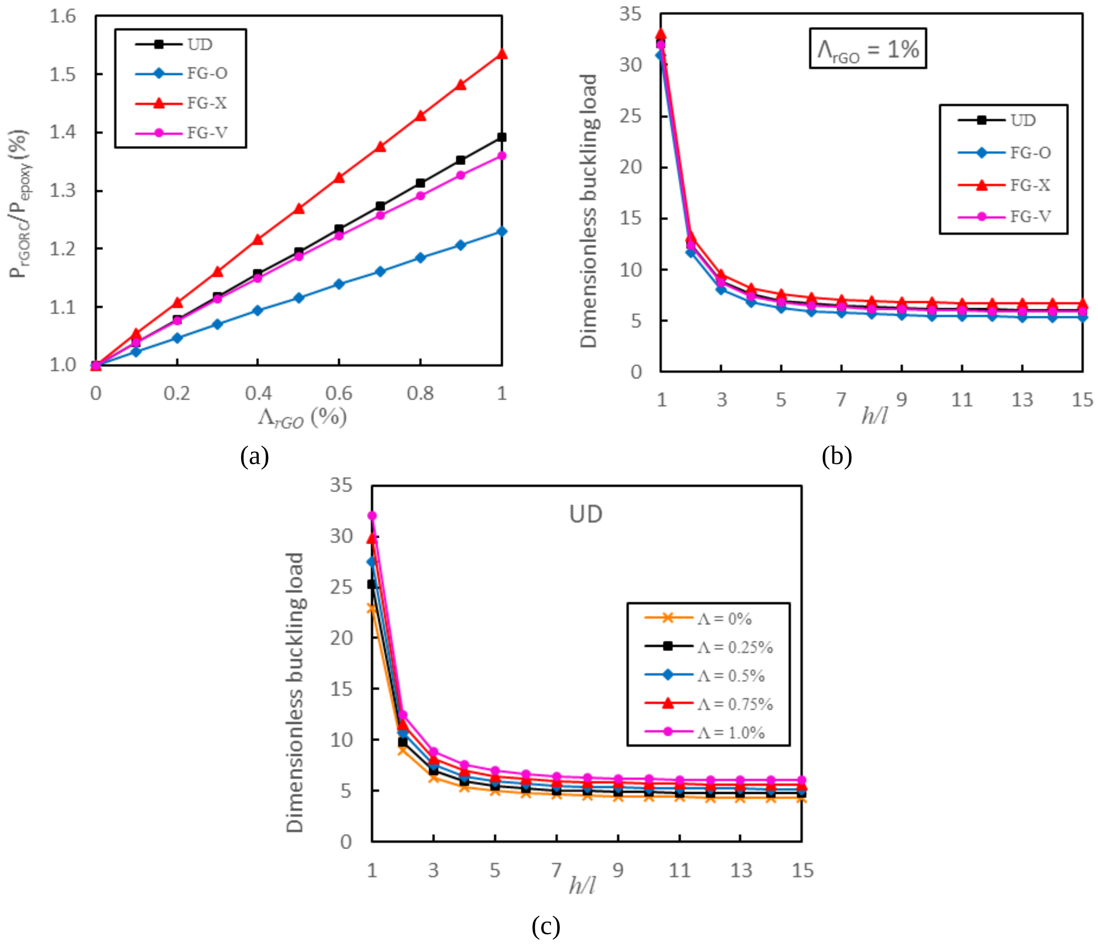

Fig. 6 Effect of rGO weight fraction on the buckling change (%) of FG rGORC plates for various distribution types (CCCC)

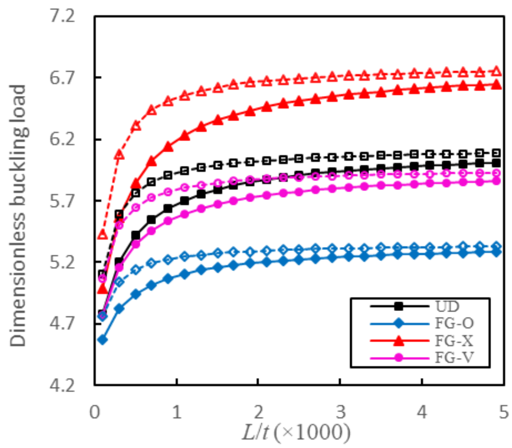

Fig. 7 Effect of *L/t* ratio on the dimensionless buckling of FG rGORC plates for various distribution types (Solid line: *W/L*=0.25, dashed line: *W/L*=1, Λ_{rGO}=1%, *l/h*=0, CCCC)

6. Conclusions

The present numerical research has studied the free vibration, and buckling of functionally graded polymer plates reinforced by reduced graphene oxide (rGO). The isogeometric analysis (IGA) and modified couple stress theory (MCST) have been used. IGA method is an efficient numerical tool for solving problems, which uses Non-Uniform Rational B-Spline (NURBS) basis functions. To determine the effective Young's modulus of reduced graphene oxide reinforced nanocomposite (rGORC), the Halpin-Tsai micromechanics scheme was applied. Furthermore, four different distribution types of rGO as well as the refined plate theory (RPT) based on Reddy's third-order function have been employed. Our results show that only a small amount of rGO significantly enhances the stiffness of composite plates due to the high Young's modulus of reduced graphene oxide. Adding only 1% of rGO into pure epoxy plates by assuming UD type results in free vibration and buckling load 18% and 39% higher as compared to epoxy, respectively. Besides, the material length scale parameter l leads to the increase of both fundamental frequency and critical buckling load. The size-dependent or length scale parameter l makes the stiffness of plates harder. For L/t beyond 2000, both fundamental frequency and critical buckling load remain almost unchanged. Moreover, among the four distribution types, FG-X and FG-O types have the most and least effects on free vibration and buckling results, respectively. Furthermore, the composite plates made of square rGO platelets (W/L=1) give a higher value for both free vibration and critical buckling load as compared to the rectangular rGO platelets (W/L=0.25).

References

Abazid, M.A., Zenkour, A.M. and Sobhy, M. (2020), "Wave propagation in FG porous GPLs-reinforced nanoplates under in-plane mechanical load and Lorentz magnetic force via a new quasi 3D plate theory", *Mech. Bas. Des. Struct. Mach*., 1-20. https://doi.org/10.1080/15397734.2020.1769651.

Akgöz, B. and Civalek, Ö. (2017), "A size-dependent beam model for stability of axially loaded carbon nanotubes surrounded by Pasternak elastic foundation", *Compos. Struct*., **176**, 1028-1038. https://doi.org/10.1016/j.compstruct.2017.06.039.

An, Y., Han, J., Zhang, X., Han, W., Cheng, Y., Hu, P. and Zhao, G. (2016), "Bioinspired high toughness graphene/ZrB2 hybrid composites with hierarchical architectures spanning several length scales", *Carbon*, **107**, 209-216. https://doi.org/10.1016/j.carbon.2016.05.074.

Arefi, M., Bidgoli, E.M. and Rabczuk, T. (2019), "Effect of various characteristics of graphene nanoplatelets on thermal buckling behavior of FGRC micro plate based on MCST", *Eur. J. Mech. A-Solid*., **77**, 103802. https://doi.org/10.1016/j.euromechsol.2019.103802.

Belmahi, S., Zidour, M. and Meradjah, M. (2019), "Small-scale effect on the forced vibration of a nano beam embedded an elastic medium using nonlocal elasticity theory", *Adv. Aircraft Spacecraft Sci*., **6**(1), 1. http://doi.org/10.12989/aas.2019.6.1.001.

Belmonte, M., Nistal, A., Boutbien, P., Román-Manso, B., Osendi, M.I. and Miranzo, P. (2016), "Toughened and strengthened silicon carbide ceramics by adding graphene-based fillers", *Scripta Mater*., **113**, 127-130. https://doi.org/10.1016/j.scriptamat.2015.10.023.

Carrera, E., de Miguel, A.G. and Pagani, A. (2017), "Extension of MITC to higher-order beam models and shear locking analysis for compact, thin-walled, and composite structures", *Int. J. Numer. Meth. Eng*., **112**(13), 1889-1908. https://doi.org/10.1002/nme.5588.

Carrera, E., Pagani, A., Petrolo, M. and Zappino, E. (2015), "Recent developments on refined theories for beams with applications", *Mech. Eng. Rev*., **2**(2), 14-00298. https://doi.org/10.1299/mer.14-00298.

Compton, O.C. and Nguyen, S.T. (2010), "Graphene oxide, highly reduced graphene oxide, and graphene:

versatile building blocks for carbon-based materials", *Small*, **6**(6), 711-723. https://doi.org/10.1002/smll.200901934.

Dastjerdi, S., Akgöz, B. and Civalek, Ö. (2020), "On the effect of viscoelasticity on behavior of gyroscopes" *Int. J. Eng. Sci*., **149**, 103236. https://doi.org/10.1016/j.ijengsci.2020.103236.

Devarajan, B. and Kapania, R.K. (2020), "Thermal buckling of curvilinearly stiffened laminated composite plates with cutouts using isogeometric analysis", *Compos. Struct.*, **238**, 111881. https://doi.org/10.1016/j.compstruct.2020.111881.

Devarajan, B. and Kapania, R.K. (2022), "Analyzing thermal buckling in curvilinearly stiffened composite plates with arbitrary shaped cutouts using isogeometric level set method", *Aerosp. Sci. Technol*., 107350. https://doi.org/10.1016/j.ast.2022.107350.

Dindarloo, M.H. and Zenkour, A.M. (2020), "Nonlocal strain gradient shell theory for bending analysis of FG spherical nanoshells in thermal environment", *Eur. Phys. J. Plus*, **135**(10), 1-18. https://doi.org/10.1140/epjp/s13360-020-00796-9.

Eringen, A.C. and Edelen, D.G.B. (1972), "On nonlocal elasticity", *Int. J. Eng. Sci.*, **10**, 233-248. https://doi.org/10.1016/0020-7225(72)90039-0.

Farzam-Rad, S.A., Hassani, B. and Karamodin, A. (2017), "Isogeometric analysis of functionally graded plates using a new quasi-3D shear deformation theory based on physical neutral surface", *Compos. Part B*, **108**, 174-189. https://doi.org/10.1016/j.compositesb.2016.09.029.

Farzam, A. and Hassani, B. (2018), "Thermal and mechanical buckling analysis of FG carbon nanotube reinforced composite plates using modified couple stress theory and isogeometric approach", *Compos. Struct*., **206**, 774-790. https://doi.org/10.1016/j.compstruct.2018.08.030.

Farzam, A. and Hassani, B. (2019a), "Size-dependent analysis of FG microplates with temperature-dependent material properties using modified strain gradient theory and isogeometric approach", *Compos. Part B*, **161**, 150-168. https://doi.org/10.1016/j.compositesb.2018.10.028.

Farzam, A. and Hassani, B. (2019b), "Isogeometric analysis of in-plane functionally graded porous microplates using modified couple stress theory", *Aerosp. Sci. Technol*., **91**, 508-524. https://doi.org/10.1016/j.ast.2019.05.012.

Farzam, A. and Hassani, B. (2019c), "A new efficient shear deformation theory for FG plates with in-plane and through-thickness stiffness variations using isogeometric approach", *Mech. Adv. Mater. Struct*., **26**(6), 512-525. https://doi.org/10.1080/15376494.2017.1400623.

Farzam, A. and Kapania, R. (2022), "Buckling analysis of functionally graded plates using Isogeometric Finite Element Method and ABAQUS", *AIAA SCITECH 2022 Forum*, San Diego. https://doi.org/10.2514/6.2022-1488.

Fenjan, R.M., Hamad, L.B. and Faleh, N.M. (2020), "Mechanical-hygro-thermal vibrations of functionally graded porous plates with nonlocal and strain gradient effects", *Adv. Aircraft Spacecraft Sci*., **7**(2), 169-86. http://doi.org/10.12989/aas.2020.7.2.169.

Fleck, N.A. and Hutchinson, J.W. (1993), "A phenomenological theory for strain gradient effects in plasticity", *J. Mech. Phys. Solid*., **41**, 1825-1857. https://doi.org/10.1016/0022-5096(93)90072-N.

Fornes, T.D. and Paul, D.R. (2003), "Modeling properties of nylon 6/clay nanocomposites using composite theories", *Polym*., **44**(17), 4993-5013. https://doi.org/10.1016/S0032-3861(03)00471-3.

García-Macías, E., Rodríguez-Tembleque, L. and Sáez, A. (2018), "Bending and free vibration analysis of functionally graded graphene vs. carbon nanotube reinforced composite plates", *Compos. Struct*., **186**, 123-138. https://doi.org/10.1016/j.compstruct.2017.11.076.

Gómez-Navarro, C., Burghard, M. and Kern, K. (2008), "Elastic properties of chemically derived single graphene sheets", *Nano Lett*., **8**(7), 2045-2049. https://doi.org/10.1021/nl801384y.

Gong, L.X., Pei, Y.B., Han, Q.Y., Zhao, L., Wu, L.B., Jiang, J.X. and Tang, L.C. (2016), "Polymer grafted reduced graphene oxide sheets for improving stress transfer in polymer composites", *Compos. Sci. Technol*., **134**, 144-152. https://doi.org/10.1016/j.compscitech.2016.08.014.

Hanzel, O., Sedlák, R., Sedláček, J., Bizovská, V., Bystrický, R., Girman, V., Kovalčíková, A., Dusza, J. and Šajgalík, P. (2017), "Anisotropy of functional properties of SiC composites with GNPs, GO and in-situ formed graphene", *J. Eur. Ceram. Soc*., **37**(12), 3731-3739.

https://doi.org/10.1016/j.jeurceramsoc.2017.03.060.
Hosseini, S.A., Moghaddam, M.H. and Rahmani, O. (2020)," Exact solution for axial vibration of the power, exponential and sigmoid FG nonlocal nanobeam", *Adv. Aircraft Spacecraft Sci.*, **7**(6), 517-36. http://doi.org/10.12989/aas.2020.7.6.517.
Huang, Y., Jiang, D., Zhang, X., Liao, Z. and Huang, Z. (2018), "Enhancing toughness and strength of SiC ceramics with reduced graphene oxide by HP sintering", *J. Eur. Ceram. Soc*., **38**(13), 4329-4337. https://doi.org/10.1016/j.jeurceramsoc.2018.05.033.
Hughes, T.J.R., Cottrell, J.A. and Bazilevs, Y. (2005), "Isogeometric analysis: CAD, finite elements, NURBS, exact geometry and mesh refinement", *Comput. Meth. Appl. Mech. Eng*., **194**, 4135-4195. https://doi.org/10.1016/j.cma.2004.10.008.
Iqbal, M.Z., Abdala, A.A., Mittal, V., Seifert, S., Herring, A.M. and Liberatore, M.W. (2016), "Processable conductive graphene/polyethylene nanocomposites: Effects of graphene dispersion and polyethylene blending with oxidized polyethylene on rheology and microstructure", *Polym*., **98**, 143-155. https://doi.org/10.1016/j.polymer.2016.06.021.
Ji, W.F., Chang, K.C., Lai, M.C., Li, C.W., Hsu, S.C., Chuang, T.L., Yeh, J.M. and Liu, W.R. (2014), "Preparation and comparison of the physical properties of PMMA/thermally reduced graphene oxides composites with different carboxylic group content of thermally reduced graphene oxides", *Compos. Part A*, **65**, 108-114. https://doi.org/10.1016/j.compositesa.2014.05.017.
Kapoor, H. and Kapania, R.K. (2012), "Geometrically nonlinear NURBS isogeometric finite element analysis of laminated composite plates", *Compos. Struct*., **94**(12), 3434-3447. https://doi.org/10.1016/j.compstruct.2012.04.028.
Kapoor, H., Kapania, R.K. and Soni, S.R. (2013), "Interlaminar stress calculation in composite and sandwich plates in NURBS Isogeometric Finite Element Analysis", *Compos. Struct*., **106**, 537-548. https://doi.org/10.1016/j.compstruct.2013.05.028.
Karami, B., Shahsavari, D., Janghorban, M. and Tounsi, A. (2019), "Resonance behavior of functionally graded polymer composite nanoplates reinforced with graphene nanoplatelets", *Int. J. Mech. Sci*., **156**, 94-105. https://doi.org/10.1016/j.ijmecsci.2019.03.036.
Kashyap, S., Pratihar, S.K. and Behera, S.K. (2016), "Strong and ductile graphene oxide reinforced PVA nanocomposites", *J. Alloy Compound*., **684**, 254-260. https://doi.org/10.1016/j.jallcom.2016.05.162.
Kiani, Y. (2018), "Isogeometric large amplitude free vibration of grapheme reinforced laminated plates in thermal environment using NURBS formulation", *Comput. Meth. Appl. Mech. Eng*., **332**, 86-101. https://doi.org/10.1016/j.cma.2017.12.015.
Kiani, Y. (2018), "NURBS-based isogeometric thermal postbuckling analysis of temperature dependent graphene reinforced composite laminated plates", *Thin Wall Struct*., **125**, 211-219. https://doi.org/10.1016/j.tws.2018.01.024.
Kim, T.A., Pyo, J.B., Lee, S.S. and Park, M. (2019), "Highly aligned and porous reduced graphene oxide structures and their application for stretchable conductors", *J. Ind. Eng. Chem*., **80**, 385-391. https://doi.org/10.1016/j.jiec.2019.08.018.
Kong, J.Y., Choi, M.C., Kim, G.Y., Park, J.J., Selvaraj, M., Han, M. and Ha, C.S. (2012), "Preparation and properties of polyimide/graphene oxide nanocomposite films with Mg ion crosslinker", *Eur. Polym. J*., **48**(8), 1394-1405. https://doi.org/10.1016/j.eurpolymj.2012.05.015.
Lam, D.C.C., Yang, F., Chong, A.C.M., Wang, J. and Tong, P. (2003), "Experiments and theory in strain gradient elasticity", *J. Mech. Phys. Solid*., **51**, 1477-1508. https://doi.org/10.1016/S0022-5096(03)00053-X.
Lee, B., Koo, M.Y., Jin, S.H., Kim, K.T. and Hong, S.H. (2014), "Simultaneous strengthening and toughening of reduced graphene oxide/alumina composites fabricated by molecular-level mixing process", *Carbon*, **78**, 212-219. https://doi.org/10.1016/j.carbon.2014.06.074.
Li, K., Wu, D., Chen, X., Cheng, J., Liu, Z., Gao, W. and Liu, M. (2018), "Isogeometric Analysis of functionally graded porous plates reinforced by graphene platelets", *Compos. Struct*., **204**, 114-130. https://doi.org/10.1016/j.compstruct.2018.07.059.
Li, Y., Tang, J., Huang, L., Wang, Y., Liu, J., Ge, X., Tjong, S.C., Li, R.K. and Belfiore, L.A. (2015a), "Facile

preparation, characterization and performance of noncovalently functionalized graphene/epoxy nanocomposites with poly (sodium 4-styrenesulfonate)", *Compos. Part A*, **68**, 1-9. https://doi.org/10.1016/j.compositesa.2014.09.016.

Li, Z., Fan, G., Tan, Z., Guo, Q., Xiong, D., Su, Y., Li, Z. and Zhang, D. (2014), "Uniform dispersion of graphene oxide in aluminum powder by direct electrostatic adsorption for fabrication of graphene/aluminum composites", *Nanotechnol*., **25**(32), 325601. https://doi.org/10.1088/0957-4484/25/32/325601.

Li, Z., Guo, Q., Li, Z., Fan, G., Xiong, D.B., Su, Y., Zhang, J. and Zhang, D. (2015b), "Enhanced mechanical properties of graphene (reduced graphene oxide)/aluminum composites with a bioinspired nanolaminated structure", *Nano Let*t., **15**(12), 8077-8083. https://doi.org/10.1021/acs.nanolett.5b03492.

Liu, J., Khan, U., Coleman, J., Fernandez, B., Rodriguez, P., Naher, S. and Brabazon, D. (2016), "Graphene oxide and graphene nanosheet reinforced aluminium matrix composites: Powder synthesis and prepared composite characteristics", *Mater. Des.*, **94**, 87-94. https://doi.org/10.1016/j.matdes.2016.01.031.

Maity, N., Mandal, A. and Nandi, A.K. (2016), "Synergistic interfacial effect of polymer stabilized graphene via non-covalent functionalization in poly (vinylidene fluoride) matrix yielding superior mechanical and electronic properties", *Polym*., **88**, 79-93. https://doi.org/10.1016/j.polymer.2016.02.028.

Miglani, J., Devarajan, B. and Kapania, R.K., (2021), "Isogeometric thermal buckling and sensitivity analysis of periodically supported laminated composite beams", *AIAA J.*, 1-10. https://doi.org/10.2514/1.J060814.

Mishra, S.K., Tripathi, S.N., Choudhary, V. and Gupta, B.D. (2014), "SPR based fibre optic ammonia gas sensor utilizing nanocomposite film of PMMA/reduced graphene oxide prepared by in situ polymerization", *Sensor Actuat. B*, **199**, 190-200. https://doi.org/10.1016/j.snb.2014.03.109.

Nguyen, L.B., Nguyen, N.V., Thai, C.H., Ferreira, A.M.J. and Nguyen-Xuan, H. (2019), "An isogeometric Bézier finite element analysis for piezoelectric FG porous plates reinforced by graphene platelets", *Compos. Struct.*, **214**, 227-245. https://doi.org/10.1016/j.compstruct.2019.01.077.

Olowojoba, G.B., Eslava, S., Gutierrez, E.S., Kinloch, A.J., Mattevi, C., Rocha, V.G. and Taylor, A.C. (2016), "In situ thermally reduced graphene oxide/epoxy composites: thermal and mechanical properties", *Appl. Nanosci*., **6**(7), 1015-1022. https://doi.org/10.1007/s13204-016-0518-y.

Pham, V.H., Dang, T.T., Hur, S.H., Kim, E.J. and Chung, J.S. (2012), "Highly conductive poly (methyl methacrylate)(PMMA)-reduced graphene oxide composite prepared by self-assembly of PMMA latex and graphene oxide through electrostatic interaction", *ACS Appl. Mater. Int*., **4**(5), 2630-2636. https://doi.org/10.1021/am300297j.

Phung-Van, P., Ferreira, A.J.M., Nguyen-Xuan, H. and Abdel Wahab, M. (2017), "An isogeometric approach for size-dependent geometrically nonlinear transient analysis of functionally graded nanoplates", *Compos. Part B*, **118**, 125-134. https://doi.org/10.1016/j.compositesb.2017.03.012.

Phung-Van, P., Thai, C.H., Nguyen-Xuan, H. and Abdel-Wahab, M. (2019), "Porosity-dependent nonlinear transient responses of functionally graded nanoplates using isogeometric analysis", *Compos. Part B*, **164**, 215-255. https://doi.org/10.1016/j.compositesb.2018.11.036.

Phung-Van, P., Thanh, C.L., Nguyen-Xuan, H. and Abdel-Wahab, M. (2018), "Nonlinear transient isogeometric analysis of FG-CNTRC nanoplates in thermal environments", *Compos. Struct.*, **201**, 882-892. https://doi.org/10.1016/j.compstruct.2018.06.087.

Potts, J.R., Lee, S.H., Alam, T.M., An, J., Stoller, M.D., Piner, R.D. and Ruoff, R.S. (2011), "Thermomechanical properties of chemically modified graphene/poly (methyl methacrylate) composites made by in situ polymerization", *Carbon*, **49**(8), 2615-2623. https://doi.org/10.1016/j.carbon.2011.02.023.

Pourjabari, A., Hajilak, Z.E., Mohammadi, A., Habibi, M. and Safarpour, H. (2019), "Effect of Porosity on free and forced vibration characteristics of the GPL reinforcement composite nanostructures", *Comput. Math. Appl*., **77**(10), 2608-2626. https://doi.org/10.1016/j.camwa.2018.12.041.

Qureshi, T.S. and Panesar, D.K. (2019), "Impact of graphene oxide and highly reduced graphene oxide on cement based composites", *Constr. Build. Mater*., **206**, 71-83. https://doi.org/10.1016/j.conbuildmat.2019.01.176.

Rafiee, M.A., Rafiee, J., Srivastava, I., Wang, Z., Song, H., Yu, Z.Z. and Koratkar, N. (2010), "Fracture and fatigue in graphene nanocomposites", *Small*, **6**, 179-183. https://doi.org/10.1002/smll.200901480.

Ramirez, C., Miranzo, P., Belmonte, M., Osendi, M.I., Poza, P., Vega-Diaz, S.M. and Terrones, M. (2014), "Extraordinary toughening enhancement and flexural strength in Si3N4 composites using graphene sheets", *J. Eur. Ceram. Soc.*, **34**(2), 161-169. https://doi.org/10.1016/j.jeurceramsoc.2013.08.039.

Reddy, J.N. (1984), "A simple higher-order theory for laminated composite plates", *J. Appl. Mech.*, **51**, 745-752. https://doi.org/10.1115/1.3167719.

Robinson, J.T., Zalalutdinov, M., Baldwin, J.W., Snow, E.S., Wei, Z., Sheehan, P. and Houston, B.H. (2008), "Wafer-scale reduced graphene oxide films for nanomechanical devices", *Nano Lett.*, **8**(10), 3441-3445. https://doi.org/10.1021/nl8023092.

Saeedi, A., Hassani, B. and Farzam, A. (2020), "Simultaneous modeling and structural analysis of curvilinearly stiffened plates using an isogeometric approach", *Acta Mechanica*, **231**(8), 3473-3498. https://doi.org/10.1007/s00707-020-02725-4.

Sahmani, S., Aghdam, M.M. and Rabczuk, T. (2018), "Nonlocal strain gradient plate model for nonlinear large-amplitude vibrations of functionally graded porous micro/nano-plates reinforced with GPLs", *Compos. Struct.*, **198**, 51-62. https://doi.org/10.1016/j.compstruct.2018.05.031.

Sandhya, P.K., Sreekala, M.S., Padmanabhan, M., Jesitha, K. and Thomas, S. (2019), "Effect of starch reduced graphene oxide on thermal and mechanical properties of phenol formaldehyde resin nanocomposites", *Compos. Part B*, **167**, 83-92. https://doi.org/10.1016/j.compositesb.2018.12.009.

She, X., He, C., Peng, Z. and Kong, L. (2014), "Molecular-level dispersion of graphene into epoxidized natural rubber: Morphology, interfacial interaction and mechanical reinforcement", *Polym.*, **55**(26), 6803-6810. https://doi.org/10.1016/j.polymer.2014.10.054.

Shin, J.H. and Hong, S.H. (2014), "Fabrication and properties of reduced graphene oxide reinforced yttria-stabilized zirconia composite ceramics", *J. Eur. Ceram. Soc.*, **34**(5), 1297-1302. https://doi.org/10.1016/j.jeurceramsoc.2013.11.034.

Sobhy, M. and Zenkour, A.M. (2019), "Porosity and inhomogeneity effects on the buckling and vibration of double-FGM nanoplates via a quasi-3D refined theory", *Compos. Struct.*, **220**, 289-303. https://doi.org/10.1016/j.compstruct.2019.03.096.

Sobhy, M. and Zenkour, A.M. (2020), "The modified couple stress model for bending of normal deformable viscoelastic nanobeams resting on visco-Pasternak foundations", *Mech. Adv. Mater. Struct.*, **27**(7), 525-538. https://doi.org/10.1080/15376494.2018.1482579.

Sobhy, M. and Zenkour, A.M., (2021), "Wave propagation in magneto-porosity FG bi-layer nanoplates based on a novel quasi-3D refined plate theory", *Wav. Rand. Complex Media*, **31**(5), 921-941. https://doi.org/10.1080/17455030.2019.1634853.

Song, M., Yang, J. and Kitipornchai, S. (2018), "Bending and buckling analyses of functionally graded polymer composite plates reinforced with graphene nanoplatelets", *Compos. Part B*, **134**, 106-113. https://doi.org/10.1016/j.compositesb.2017.09.043.

Starkova, O., Chandrasekaran, S., Prado, L.A., Tölle, F., Mülhaupt, R. and Schulte, K. (2013), "Hydrothermally resistant thermally reduced graphene oxide and multi-wall carbon nanotube based epoxy nanocomposites", *Polym. Degrad. Stabil.*, **98**(2), 519-526. https://doi.org/10.1016/j.polymdegradstab.2012.12.005.

Suk, J.W., Piner, R.D., An, J. and Ruoff, R.S. (2010), "Mechanical properties of monolayer graphene oxide", *ACS Nano*, **4**(11), 6557-6564. https://doi.org/10.1021/nn101781v.

Thai, C.H., Ferreira, A.J., Tran, T.D. and Phung-Van, P. (2019b), "A size-dependent quasi-3D isogeometric model for functionally graded graphene platelet-reinforced composite microplates based on the modified couple stress theory", *Compos. Struct.*, **234**, 111695. https://doi.org/10.1016/j.compstruct.2019.111695.

Thai, C.H., Ferreira, A.J.M. and Phung-Van, P. (2019a), "Size dependent free vibration analysis of multilayer functionally graded GPLRC microplates based on modified strain gradient theory", *Compos. Part B*, **169**, 174-188. https://doi.org/10.1016/j.compositesb.2019.02.048.

Thai, C.H., Ferreira, A.J.M., Rabczuk, T. and Nguyen-Xuan, H. (2017), "A naturally stabilized nodal integration meshfree formulation for carbon nanotube-reinforced composite plate analysis", *Eng. Anal. Bound. Elem.*, **160**, 689-705. https://doi.org/10.1016/j.enganabound.2017.10.018.

Thai, C.H., Ferreira, A.J.M., Tran, T.D. and Phung-Van, P. (2019c), "Free vibration, buckling and bending analyses of multilayer functionally graded graphene nanoplatelets reinforced composite plates using the

NURBS formulation", *Compos. Struct.*, **220**, 749-759. https://doi.org/10.1016/j.compstruct.2019.03.100.

Thai, H.T. and Kim, S.E. (2013), "A size-dependent functionally graded Reddy plate model based on a modified couple stress theory", *Compos. Part B*, **45**, 1636-1645. https://doi.org/10.1016/j.compositesb.2012.09.065.

Thanh, C.L., Phung-Van, P., Thai, C.H., Nguyen-Xuan, H. and Abdel Wahab, M. (2018), "Isogeometric analysis of functionally graded carbon nanotube reinforced composite nanoplates using modified couple stress theory", *Compos. Struct.*, **184**, 633-649. https://doi.org/10.1016/j.compstruct.2017.10.025.

TK, B.S., Nair, A.B., Abraham, B.T., Beegum, P.S. and Thachil, E.T. (2014), "Microwave exfoliated reduced graphene oxide epoxy nanocomposites for high performance applications", *Polym.*, **55**(16), 3614-3627. https://doi.org/10.1016/j.polymer.2014.05.032.

Tripathi, S.N., Saini, P., Gupta, D. and Choudhary, V. (2013), "Electrical and mechanical properties of PMMA/reduced graphene oxide nanocomposites prepared via in situ polymerization", *J. Mater. Sci.*, **48**(18), 6223-6232. https://doi.org/10.1007/s10853-013-7420-8.

Van Es, M.A. (2001), "Polymer-clay nanocomposites: the importance of particle dimensions", Ph.D. Thesis, Delft University of Technology, Delft, The Netherlands.

Walker, L.S., Marotto, V.R., Rafiee, M.A., Koratkar, N. and Corral, E.L. (2011), "Toughening in graphene ceramic composites", *ACS Nano*, **5**(4), 3182-3190. https://doi.org/10.1021/nn200319d.

Wang, J., Shi, Z., Ge, Y., Wang, Y., Fan, J. and Yin, J. (2012), "Solvent exfoliated graphene for reinforcement of PMMA composites prepared by in situ polymerization", *Mater. Chem. Phys.*, **136**(1), 43-50. https://doi.org/10.1016/j.matchemphys.2012.06.017.

Weon, J.I. (2009), "Mechanical and thermal behavior of polyamide-6/clay nanocomposite using continuum-based micromechanical modeling", *Macromol. Res.*, **17**(10), 797-806. https://doi.org/10.1007/BF03218617.

Xia, H., Zhang, X., Shi, Z., Zhao, C., Li, Y., Wang, J. and Qiao, G. (2015), "Mechanical and thermal properties of reduced graphene oxide reinforced aluminum nitride ceramic composites", *Mater. Sci. Eng.*, **639**, 29-36. https://doi.org/10.1016/j.msea.2015.04.091.

Xu, C., Gao, J., Xiu, H., Li, X., Zhang, J., Luo, F., Zhang, Q., Chen, F. and Fu, Q. (2013), "Can in situ thermal reduction be a green and efficient way in the fabrication of electrically conductive polymer/reduced graphene oxide nanocomposites?", *Compos. Part A*, **53**, 24-33. https://doi.org/10.1016/j.compositesa.2013.06.007.

Yang, F., Chong, A.C.M., Lam, D.C.C. and Tong, P. (2002), "Couple stress based strain gradient theory for elasticity", *Int. J. Solids Struct.*, **39**, 2731-2743. https://doi.org/10.1016/S0020-7683(02)00152-X.

Yousefi, N., Gudarzi, M.M., Zheng, Q., Lin, X., Shen, X., Jia, J., Sharif, F. and Kim, J.K. (2013b), "Highly aligned, ultralarge-size reduced graphene oxide/polyurethane nanocomposites: mechanical properties and moisture permeability", *Compos. Part A*, **49**, 42-50. https://doi.org/10.1016/j.compositesa.2013.02.005.

Yousefi, N., Lin, X., Zheng, Q., Shen, X., Pothnis, J.R., Jia, J., Zussman, E. and Kim, J.K. (2013a), "Simultaneous in situ reduction, self-alignment and covalent bonding in graphene oxide/epoxy composites", *Carbon*, **59**, 406-417. https://doi.org/10.1016/j.carbon.2013.03.034.

Zeng, X., Yang, J. and Yuan, W. (2012), "Preparation of a poly (methyl methacrylate)-reduced graphene oxide composite with enhanced properties by a solution blending method", *Eur. Polym. J.*, **48**(10), 1674-1682. https://doi.org/10.1016/j.eurpolymj.2012.07.011.

Zenkour, A. M. (2018b), "Refined two-temperature multi-phase-lags theory for thermomechanical response of microbeams using the modified couple stress analysis", *Acta Mechanica*, **229**(9), 3671-3692. https://doi.org/10.1007/s00707-018-2172-9.

Zenkour, A.M. (2018a), "Modified couple stress theory for micro-machined beam resonators with linearly varying thickness and various boundary conditions", *Arch. Mech. Eng.*, **65**(1), 43-64. https://doi.org/10.24425/119409.

Zhang, L.W., Liew, K.M. and Reddy, J.N. (2016), "Postbuckling of carbon nanotube reinforced functionally graded plates with edges elastically restrained against translation and rotation under axial compression", *Comput. Meth. Appl. Mech. Eng.*, **298**, 1-28. https://doi.org/10.1016/j.cma.2015.09.016.

Zhang, Z., Li, Y., Wu, H., Zhang, H., Wu, H., Jiang, S. and Chai, G. (2018), "Mechanical analysis of functionally graded graphene oxide-reinforced composite beams based on the first-order shear deformation theory", *Mech. Adv. Mat. Struct.*, 1-9. https://doi.org/10.1080/15376494.2018.1444216.

Zhao, J., Wang, Q., Deng, X., Choe, K., Zhong, R. and Shuai, C. (2019), "Free vibrations of functionally graded porous rectangular plate with uniform elastic boundary conditions", *Compos. Part B*, **168**, 106-120. https://doi.org/10.1016/j.compositesb.2018.12.044.

Zhou, T., Chen, F., Tang, C., Bai, H., Zhang, Q., Deng, H. and Fu, Q. (2011), "The preparation of high performance and conductive poly (vinyl alcohol)/graphene nanocomposite via reducing graphite oxide with sodium hydrosulfite", *Compos. Sci. Technol.*, **71**(9), 1266-1270. https://doi.org/10.1016/j.compscitech.2011.04.016.

Zhu, Y., Murali, S., Cai, W., Li, X., Suk, J.W., Potts, J.R. and Ruoff, R.S. (2010), "Graphene and graphene oxide: synthesis, properties, and applications", *Adv. Mater.*, **22**(35), 3906-3924. https://doi.org/10.1002/adma.201001068.

EC